Transient analysis for the cathode gas diffusion layer of PEM fuel cells

Datong Song, Qianpu Wang, Zhong-Sheng Liu*, Cheng Huang

Institute for Fuel Cell Innovation, National Research Council, 3250 East Mall, Vancouver, BC, Canada V6T 1W5

Abstract

A one-dimensional, non-isothermal, two-phase transient model has been developed to study the transient behaviour of water transport in the cathode gas diffusion layer of PEM fuel cells. The effects of four parameters, namely the liquid water saturation at the interface of the gas diffusion layer and flow channels, the proportion of liquid water to all of the water at the interface of the cathode catalyst layer and the gas diffusion layer, the current density, and the contact or wetting angle, on the transient distribution of liquid water saturation in the cathode gas diffusion layer are investigated. Especially, the time needed for liquid water saturation to reach steady state and the liquid water saturation at the interface of the cathode catalyst layer and gas diffusion layer are plotted as functions of the above four parameters. The ranges of water vapour condensation and liquid water evaporation are identified across the thickness of the gas diffusion layer. In addition, the effects of the above four parameters on the steady state distributions of gas phase pressure, water vapour concentration, oxygen concentration and temperature are also presented. It is found that increasing any one of the first three parameters will increase the water saturation at the interface of the catalyst layer and gas diffusion layer, but decrease the time needed for the liquid water saturation to reach steady state. When the liquid water saturation at the interface of the gas diffusion layer and flow channels is high enough (≥ 0.1), the liquid water saturation at steady state is almost uniformly distributed across the thickness of the gas diffusion layer. It is also found that, under the given initial and boundary conditions in this paper, evaporation takes place within the gas diffusion layer close to the channel side and is the major process for water phase change at low current density ($<2000\,\mathrm{A\,m^{-2}}$); condensation occurs close to the catalyst layer side within the gas diffusion layer and dominates the phase change at high current density ($>5000\,\mathrm{A\,m^{-2}}$). For hydrophilic gas diffusion layers, both the time needed for liquid water saturation to reach steady state and the water saturation at the interface of the catalyst layer and gas diffusion layer will increase when the contact angle increases; but for hydrophobic gas diffusion layers, both of them decrease when the contact angle increases.

© 2005 Elsevier B.V. All rights reserved.

Keywords: Two-phase transport; Transient analysis; PEM fuel cell; Gas diffusion layer

1. Introduction

Polymer electrolyte membrane (PEM) fuel cells have been demonstrated as a promising alternative power source for portable, automotive, and stationary applications. In order to commercialize PEM fuel cells several technological problems have to be overcome. Water management is one of the most critical and challenging problems because insufficient amount of liquid water reduces significantly proton conductivity and too much water hinders the reactants coming through the gas diffusion layer (GDL) to the reaction sites in the catalyst layer (CL)

causing mass transport limitation. A fine balance of liquid water can only be established based on a better understanding of water transport phenomena.

In the past decade, two-phase mathematical models for PEM fuel cells or their cathodes have been published [1–15]. He et al. [1] proposed a two-dimensional, two-phase, steady-state, isothermal model for evaluating the effects of liquid water transport on the performance of the cathodes of PEM fuel cells with interdigitated flow fields. An interfacial mass transfer rate was introduced in their model to describe the mass change between the gas phase and liquid phase of water. Later, Lin et al. [2] further refined above model by incorporating a thin film-agglomerate model for catalyst layers. Janssen [3] presented a steady state, two-phase and two-dimensional model for PEM fuel cells based on the concentrated solution theory. Wang et al. [4] developed a two-dimensional, isothermal model for the

* Corresponding author. Tel.: +1 604 221 3068.
  E-mail addresses: datong.song@nrc.gc.ca (D. Song), simon.liu@nrc.gc.ca (Z.-S. Liu).

Nomenclature

c_i	specific heat capacity of phase i (J kg^{-1} K^{-1})
C_i^j	mass fraction of species j in phase i
D_i^j	bulk diffusion coefficient of species j in phase i (m^2 s^{-1})
$D_{i,\text{eff}}^j$	effective diffusion coefficient of species j in phase i (m^2 s^{-1})
F	Faraday's constant (C mol^{-1})
H_{vap}	enthalpy of vaporization of water (J kg^{-1})
i_c	current density (A m^{-2})
$J(s)$	Leverett function
k_{cond}	water vapour condensation rate (s^{-1})
k_i	thermal conductivity in phase i (W m^{-1} K^{-1})
k_i^j	thermal conductivity of species j in phase i (W m^{-1} K^{-1})
k_{ri}	relative permeability of phase i
k_{vap}	liquid water evaporation rate (N^{-1} m^2 s^{-1})
K	permeability of the GDL (m^2)
L	thickness of the cathode GDL (m)
$m^{\text{H}_2\text{O}}$	interfacial mass transfer rate of water (kg m^{-3} s^{-1})
M_g	average molar mass of the gas phase (kg mol^{-1})
M^j	molar mass of species j (kg mol^{-1})
p_c	capillary pressure (N m^{-2})
p_i	pressure in phase i (N m^{-2})
R	gas constant (J mol^{-1} K^{-1})
RH	relative humidity
s	liquid water saturation
t	time coordinate (s)
t_{steady}	time needed for water saturation to reach steady state
T	temperature (K)
u_i	velocity in phase i (m s^{-1})
x	position coordinate (m)
x_i^j	molar fraction of species j in phase i
$x_{\text{sat}}^{\text{H}_2\text{O}}$	saturation molar fraction of water vapour

Greek symbols

α	net drag coefficient in the membrane
β	proportion factor
ΔS_c^{Pt}	entropy production for the cathode (J mol^{-1} K^{-1})
Δt	time step used in the numerical simulation
ε	porosity of the cathode GDL
ζ_1, ζ_2	parameters in current density expression (Eq. (42)) (A m^{-2} V^{-1})
η_c	overpotential in the cathode catalyst layer
θ_c	contact or wetting angle
μ_i	dynamic viscosity of phase i (kg m^{-1} s^{-1})
ρ_i	density of phase i (kg m^{-3})
σ	surface tension (N m^{-1})
σ_c	electric conductivity of solid phase (S m^{-1})

Subscripts

c	cathode, capillary, or contact
cond	condensation
eff	effective value of a parameter
g	gas phase
j	species index
l	liquid phase
L	at $x = L$
r	relative
s	solid phase
sat	saturation
steady	at steady state
vap	vaporization
0	at $x = 0$ or $t = 0$

Superscripts

H_2O	water
i	phase index
N_2	nitrogen
O_2	oxygen
Pt	platinum

air cathode of PEM fuel cells based on the multiphase mixture formulation developed by Wang and Cheng [5]. The single- and two-phase regimes for the water distribution and transport are classified by the threshold current density corresponding to the first appearance of liquid water at the membrane/cathode interface. A similar model was published by You and Liu [6] to study the effects of operating parameters on the two-phase mass transport in the cathode of PEM fuel cells. Mazumder and Cole [7] proposed a three-dimensional, isothermal mathematical model for PEM fuel cells to predict the liquid water transport where the water phase change was expressed by the same way as in [1,2]. Berning and Djilali [8] also developed a three-dimensional, two-phase model for the cathode and anode of PEM fuel cells, and overall water condensation in both cathode and anode was predicted.

All of above mentioned two-phase models assumed that the GDL is completely hydrophilic (zero contact angle). In addition, they are mainly steady state and isothermal models. The liquid water transport in a hydrophobic GDL was explained by Nam and Kaviany in their one-dimensional, two-phase model [9]. Recently, Pasaogullari and Wang [10] extended the model proposed in [4] to account for both wetting properties, hydrophilicity and hydrophobicity, of GDLs. Weber et al. [11] discussed the effect of the hydrophilicity or hydrophobicity of GDLs on the cell performance through a one-dimensional, two-phase, steady-state model. The same issue was also addressed in the work published by Pasaogullari and Wang [12].

Water phase change in PEM fuel cells depends on pressure and temperature as well. A temperature difference $\sim$6 °C at 1 A cm^{-2} along the MEA thickness was predicted and validated by the non-isothermal and two-phase PEM fuel cell model devel-

oped by Noponen et al. [13], in which the contact resistance for both heat transfer and electric current were considered. Based on this model, Birgersson et al. [14] compared the simulation results between the two different expressions of the capillary pressure, one was given by Wang et al. [4] and the other was defined by Natarajan and Nguyen [15].

The transient analysis of water transport through fuel cells is needed when we deal with the rapid variation of loads [16], which is relevant to automotive applications. Unfortunately, only few open reports [16–19] can be found on this issue. Ceraolo et al. [16] investigated the static and dynamic behaviour of cell voltage of PEM fuel cells through a one-dimensional, single phase, isothermal model. Amphlett et al. [17] gave an analytical model to predict the transient responses of a PEM fuel cell stack during start-up, load step-up and shut-down. Natarajan and Nguyen [15] developed a two-dimensional, two-phase, transient model for the cathode of PEM fuel cells with conventional gas distributors and the transient profiles of oxygen concentration, local current density, and liquid water saturation were presented. But their model did not consider the temperature change in the cell and therefore was isothermal. This model was later expanded to a pseudo-three-dimensional one [18] to account for the dimension along with the channel direction but only steady state analysis was conducted there. Recently, Wang and Wang [19] published a three-dimensional, isothermal transient model to study the transient dynamics of PEM fuel cell operation and concluded that the time for fuel cell to reach steady state is in the order of 10 s due to the effect of water accumulation in the membrane. Gas transport reaches steady state after 0.1 s. Unfortunately it is a single-phase, isothermal model and cannot predict liquid water transport.

The purpose of this paper is to investigate the transient behaviours of liquid water transport in the cathode GDL of PEM fuel cells by means of a one-dimensional, two-phase, non-isothermal model. It can determine where the phase change takes place in the cathode GDL and under what conditions. A parameter is adopted to account for the proportion of liquid water to all of the water introduced by electro-osmotic drag and the electrochemical reaction in the cathode CL at the cathode CL/GDL interface. The effects of this parameter, as well as other three parameters (the liquid water saturation at the interface of GDL/channels, the working current density, and the wetting or contact angle) on the transient and steady state behaviour of liquid water are presented and discussed.

2. Mathematical model

2.1. Basic equations

The classical multiphase approach developed by Abriola and Pinder [20] provides a full system of governing equations for velocities, scalar pressures, scalar liquid saturations, mass concentrations, and temperature. The governing equations were summarized in [5].

A schematic of the cathode gas diffusion layer (GDL) of a PEM fuel cell is given in Fig. 1. Applying above multiphase model to the cathode GDL where three species (water, oxygen
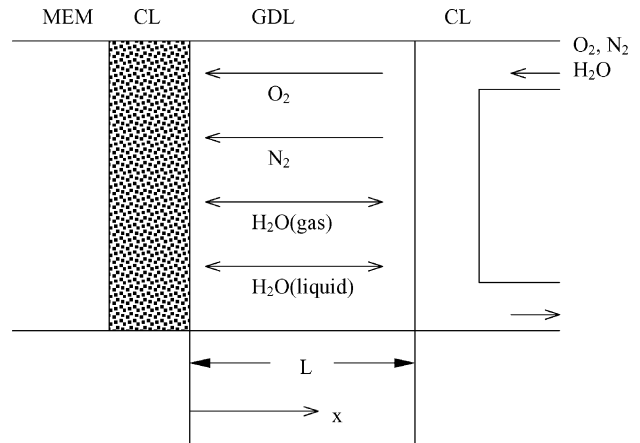

Fig. 1. The schematic of a cathode GDL of a PEM fuel cell.

and nitrogen) and two phases (liquid and gas) exist, the governing equations can be obtained as follows.

(i) Mass conservation of phases

The mass balance in each phase is considered separately.
  In the liquid phase

$$\varepsilon \frac{\partial(\rho_l s)}{\partial t} + \frac{\partial(\rho_l u_l)}{\partial x} = m^{H_2O} \tag{1}$$

where ε is the GDL porosity, ρ_l is the liquid water density, s is the liquid water saturation, u_l is the liquid water velocity, m^{H_2O} is the interfacial mass transfer rate of water from vapour phase to liquid phase, and t and x are the time and position coordinates, respectively.
  In the gas phase

$$\varepsilon \frac{\partial(\rho_g(1-s))}{\partial t} + \frac{\partial(\rho_g u_g)}{\partial x} = -m^{H_2O} \tag{2}$$

here ρ_g and u_g are the gas density and velocity, respectively.

(ii) Momentum conservation

The momentum conservations for the liquid phase and the gas phase are described by Darcy's law.
  In the liquid phase

$$u_l = -\frac{K k_{rl}}{\mu_l} \frac{\partial p_l}{\partial x} \tag{3}$$

In the gas phase

$$u_g = -\frac{K k_{rg}}{\mu_g} \frac{\partial p_g}{\partial x} \tag{4}$$

where K is the absolute permeability of the GDL, k_{rl} and k_{rg} are the relative permeabilities of liquid phase and gas phase, respectively, μ_l and μ_g are the dynamic viscosities of liquid phase and gas phase, respectively, and p_l and p_g denote the partial pressure of liquid phase and gas phase, respectively.

The difference between the gas phase pressure and liquid phase pressure is known as capillary pressure,

$$p_c = p_g - p_l \tag{5}$$

(iii) Mass conservation of species

Water in the liquid phase

$$\varepsilon \frac{\partial}{\partial t}(\rho_l s C_l^{H_2O}) + \frac{\partial}{\partial x}(\rho_l u_l C_l^{H_2O})$$
$$= -\frac{\partial}{\partial x}\left(-\varepsilon \rho_l s D_l^{H_2O} \frac{\partial C_l^{H_2O}}{\partial x}\right) + J^{H_2O} \tag{6}$$

Water in the gas phase

$$\varepsilon \frac{\partial}{\partial t}(\rho_g(1-s)C_g^{H_2O}) + \frac{\partial}{\partial x}(\rho_g u_g C_g^{H_2O})$$
$$= -\frac{\partial}{\partial x}\left(-\varepsilon \rho_g(1-s)D_g^{H_2O} \frac{\partial C_g^{H_2O}}{\partial x}\right) - J^{H_2O} \tag{7}$$

where $C_l^{H_2O}$ and $C_g^{H_2O}$ stand for the mass concentration of water in the liquid phase and in the gas phase, respectively, and $D_l^{H_2O}$ and $D_g^{H_2O}$ are the diffusion coefficients of water in the liquid phase and in the gas phase respectively. The term, J^{H_2O}, denotes the interphase species transfer rate caused by chemical nonequilibrium and/or phase change at the interfaces between the liquid phase and gas phase.

Oxygen

Because there is no phase change, the mass conservation equation for oxygen is given only in the gas phase

$$\varepsilon \frac{\partial}{\partial t}(\rho_g(1-s)C_g^{O_2}) + \frac{\partial}{\partial x}(\rho_g u_g C_g^{O_2})$$
$$= -\frac{\partial}{\partial x}\left(-\varepsilon \rho_g(1-s)D_g^{O_2} \frac{\partial C_g^{O_2}}{\partial x}\right) \tag{8}$$

where $C_g^{O_2}$ is the mass concentration of oxygen in the gas phase, and $D_g^{O_2}$ is the diffusion coefficient of oxygen in the gas phase.

(iv) Energy conservation

In GDLs, energy is transferred in three phases, liquid phase, gas phase and solid phase. The conservation equation in each phase is given as follows.

In the liquid phase

$$\varepsilon \frac{\partial}{\partial t}(\rho_l s h_l) + \frac{\partial}{\partial x}(\rho_l u_l h_l) = \frac{\partial}{\partial x}\left(s k_l \frac{\partial T}{\partial x}\right) + q_l \tag{9}$$

In the gas phase

$$\varepsilon \frac{\partial}{\partial t}(\rho_g(1-s)h_g) + \frac{\partial}{\partial x}(\rho_g u_g h_g) = \frac{\partial}{\partial x}\left((1-s)k_g \frac{\partial T}{\partial x}\right) + q_g \tag{10}$$

In the solid phase

$$(1-\varepsilon)\frac{\partial}{\partial t}(\rho_s h_s) = \frac{\partial}{\partial x}\left(k_s \frac{\partial T}{\partial x}\right) + q_s \tag{11}$$

where local thermal equilibrium among phases has been assumed ($T_l = T_g = T_s = T$), k_l, k_g and k_s represent the effective thermal conductivities of liquid phase, gas phase and solid phase,

respectively, and q_l, q_g and q_s are the interphase heat fluxes associated with liquid phase, gas phase and solid phase, respectively.

The phase enthalpies, h_l, h_g and h_s, are related to the common temperature T via

$$h_l = \int_0^T c_l \, dT + h_l^0 \tag{12}$$

$$h_g = \int_0^T c_g \, dT + h_g^0 \tag{13}$$

$$h_s = \int_0^T c_s \, dT + h_s^0 \tag{14}$$

where c_l, c_g and c_s represent the effective specific heat capacities of liquid phase, gas phase and solid phase, respectively, h_l^0, h_g^0 and h_s^0 are the enthalpies at absolute zero in three phases, respectively.

2.2. Transformed equations with initial and boundary conditions

The above basic conservation laws provide a full system of governing equations for the unknown velocities (u_l and u_g), pressures (p_l and p_g), the liquid saturation (s), mass concentrations ($C_g^{H_2O}$ and $C_g^{O_2}$), and the common temperature (T).

In order to solve the unknowns effectively, the above governing equations are simplified and transformed into the following forms.

2.2.1. Liquid water transport

Substituting the momentum conservation equation for liquid water, Eq. (3), into Eq. (1) and noting that the partial pressure in the liquid phase can be expressed into the difference between the gas phase pressure and capillary pressure through Eq. (5), the governing equation for the liquid water saturation can be rewritten as

$$\varepsilon \rho_l \frac{\partial s}{\partial t} + \frac{\partial}{\partial x}\left[\rho_l \frac{Kk_{rl}}{\mu_l} \frac{dp_c}{ds} \frac{\partial s}{\partial x} - \rho_l \frac{Kk_{rl}}{\mu_l} \frac{\partial p_g}{\partial x}\right] = m^{H_2O} \tag{15}$$

with the following initial and boundary conditions

$$s|_{t=0} = s_0 \tag{16}$$

$$-\left[\rho_l \frac{Kk_{rl}}{\mu_l} \frac{dp_c}{ds} \frac{\partial s}{\partial x} - \rho_l \frac{Kk_{rl}}{\mu_l} \frac{\partial p_g}{\partial x}\right]\Bigg|_{x=0} = \beta \frac{i_c}{4F}(2+4\alpha)M^{H_2O} \tag{17}$$

$$s|_{x=L} = s_L \tag{18}$$

where s_0 and s_L are given liquid water saturations, i_c is the current density, F is the Faraday's constant, M^{H_2O} is the molar mass of water, α is the net drag coefficient, including both the electro-osmotic drag and back diffusion in the membrane.

A parameter, denoted by β ($0 \le \beta \le 1$), is employed in Eq. (17) to account for the liquid water fraction to the total amount of water (including water vapour) at the interface of cathode CL/GDL, which is introduced by the electro-osmotic drag and the electrochemical reaction in the cathode catalyst layer.

2.2.2. Gas transport

The gas phase transport is characterized by its partial pressure and the governing equation can be obtained as following: Assuming that the gas phase obeys the ideal gas law, so the gas density is given by

$$\rho_g = \frac{p_g M_g}{RT} \tag{19}$$

where M_g is the molar mass of the gas mixture, R is the gas constant and T is the common temperature.

Substituted from Eqs. (1), (4) and (19), Eq. (2) can be converted into a differential equation of the gas phase pressure

$$\varepsilon(1-s)\frac{M_g}{RT}\frac{\partial p_g}{\partial t} + \frac{\partial}{\partial x}\left[-\frac{Kk_{rg}}{\mu_g}\frac{p_g M_g}{RT}\frac{\partial p_g}{\partial x}\right]$$
$$+ \frac{1}{\rho_l}\left[\rho_l \frac{\partial u_l}{\partial x} - m^{H_2O}\right]\frac{M_g}{RT}p_g = -m^{H_2O} \tag{20}$$

with the following initial and boundary conditions

$$p_g|_{t=0} = p_{g,L} \tag{21}$$

$$\left[\frac{Kk_{rg}}{\mu_g}\frac{p_g M_g}{RT}\frac{\partial p_g}{\partial x}\right]\Bigg|_{x=0}$$
$$= -\frac{i_c}{4F}M^{O_2} + (1-\beta)\frac{i_c}{4F}(2+4\alpha)M^{H_2O} \tag{22}$$

$$p_g|_{x=L} = p_{g,L} \tag{23}$$

here M^{O_2} is the molar mass of oxygen.

2.2.3. Water vapour transport

The liquid water density is assumed constant because its variation in the temperature interval of 300–363 K is less than $O(10^{-2})$ [14]. The concentration or mass fraction for liquid water is 1. So both the spatial and temporal derivatives of liquid water concentration are 0. Eq. (6) is reduced to

$$m^{H_2O}C_l^{H_2O} = J^{H_2O} \tag{24}$$

Using Eq. (7), the governing equation for water vapour transport is derived as

$$\varepsilon\rho_g(1-s)\frac{\partial C_g^{H_2O}}{\partial t} + \frac{\partial}{\partial x}\left[-\varepsilon\rho_g(1-s)D_{g,eff}^{H_2O}\frac{\partial C_g^{H_2O}}{\partial x} + \rho_g u_g C_g^{H_2O}\right]$$
$$- \left[\frac{\partial(\rho_g u_g)}{\partial x} + m^{H_2O}\right]C_g^{H_2O} = -m^{H_2O}C_l^{H_2O} \tag{25}$$

with the following initial and boundary conditions

$$C_g^{H_2O}|_{t=0} = C_{g,L}^{H_2O} \tag{26}$$

$$-\left[-\varepsilon\rho_g(1-s)D_{g,eff}^{H_2O}\frac{\partial C_g^{H_2O}}{\partial x} + \rho_g u_g C_g^{H_2O}\right]\Bigg|_{x=0}$$
$$= (1-\beta)\frac{i_c}{4F}(2+4\alpha)M^{H_2O} \tag{27}$$

$$C_g^{H_2O}|_{x=L} = C_{g,L}^{H_2O} \tag{28}$$

where $D_{g,eff}^{H_2O}$ is the effective diffusion coefficient of water vapour.

2.2.4. Oxygen transport

Due to the low solubility of oxygen in liquid water, the oxygen concentration in liquid water is neglected [6]. The governing equation for oxygen transport is,

$$\varepsilon\rho_g(1-s)\frac{\partial C_g^{O_2}}{\partial t} + \frac{\partial}{\partial x}\left[-\varepsilon\rho_g(1-s)D_{g,eff}^{O_2}\frac{\partial C_g^{O_2}}{\partial x} + \rho_g u_g C_g^{O_2}\right]$$
$$- \left[\frac{\partial(\rho_g u_g)}{\partial x} + m^{H_2O}\right]C_g^{O_2} = 0 \tag{29}$$

here $D_{g,eff}^{O_2}$ is the effective diffusion coefficient of oxygen.

The initial and boundary conditions for Eq. (29) are

$$C_g^{O_2}|_{t=0} = C_{g,L}^{O_2} \tag{30}$$

$$-\left[-\varepsilon\rho_g(1-s)D_{g,eff}^{O_2}\frac{\partial C_g^{O_2}}{\partial x} + \rho_g u_g C_g^{O_2}\right]\Bigg|_{x=0} = -\frac{i_c}{4F}M^{O_2} \tag{31}$$

$$C_g^{O_2}|_{L=0} = C_{g,L}^{O_2} \tag{32}$$

2.2.5. Heat transfer

Differentiating Eqs. (9)–(11), rearranging the resultant three equations based on Eqs. (1) and (2), and summating them together, the final energy conservation equation becomes

$$[\varepsilon\rho_l s c_l + \varepsilon\rho_g(1-s)c_g + (1-\varepsilon)\rho_s c_s]\frac{\partial T}{\partial t}$$
$$+ \frac{\partial}{\partial x}\left[-(sk_l + (1-s)k_g + k_s)\frac{\partial T}{\partial x}\right]$$
$$+ [\rho_l u_l c_l + \rho_g u_g c_g]\frac{\partial T}{\partial x} = H_{vap}m^{H_2O} + q \tag{33}$$

where

$$H_{vap} = h_g - h_l \tag{34}$$

is the enthalpy of water vaporization and generally is a function of temperature.

The external volumetric heat or sink source here comes from the conduction current and is given as

$$q = q_l + q_g + q_s = \sigma_c\left(\frac{i_c}{\sigma_c}\right)^2 \tag{35}$$

where σ_c is the electric conductivity of solid phase.

Initial condition and boundary conditions for Eq. (33) are

$$T|_{t=0} = T_L \tag{36}$$

$$\left[(sk_l + (1-s)k_g + k_s)\frac{\partial T}{\partial x}\right]\Bigg|_{x=0} = i_c\left(-\frac{T|_{x=0}\Delta S_c^{Pt}}{4F} - \eta_c\right) \tag{37}$$

$$T|_{x=L} = T_L \tag{38}$$

where ΔS_c^{Pt} is the entropy production for the cathode [13,14,21]. η_c is the overpotential in the cathode catalyst layer and related to the cathode current density (i_c) by [14]

$$i_c = \zeta_1((1-s)x_g^{O_2})|_{x=0}\exp(-\zeta_2\eta_c) \tag{39}$$

where ζ_1 and ζ_2 are two parameters adopted from [13,14], $x_g^{O_2}$ is the molar fraction of oxygen.

2.3. Parameter expressions and constitutive relations

The complexity and difficulty of the numerical analysis for the multiphase transport through porous GDL arise from the fact that the porous GDL properties such as relative permeability, dynamic viscosity and capillary pressure depend upon liquid water saturation and temperature. To complete the needed numerical study, some empirical or fitted parameters or constitute relations are employed and listed here.

Relative permeabilities of liquid phase and gas phase are related to the liquid water saturation by [4],

$$k_{\text{rl}} = s^3 \tag{40}$$

$$k_{\text{rg}} = (1-s)^3 \tag{41}$$

The dynamic viscosity of liquid phase depends on temperature [14],

$$\mu_l = 0.6612(T-229)^{-1.562} \tag{42}$$

The capillary pressure expression is adopted from [10],

$$p_c = \sigma\cos(\theta_c)\left(\frac{\varepsilon}{K}\right)^{1/2}J(s) \tag{43}$$

where σ is the surface tension, θ_c is the contact or wetting angle, $J(s)$ is the Leverett function and given for both hydrophilic and hydrophobic porous media as follows,

$$J(s) = \begin{cases} 1.417(1-s) - 2.210(1-s)^2 + 1.263(1-s)^3 & \text{if } \theta_c < 90° \\ 1.417s - 2.210s^2 + 1.263s^3 & \text{if } \theta_c > 90° \end{cases} \tag{44}$$

The interfacial mass transfer rate of water between the gas phase and the liquid phase is given by [1,9,14,15]

$$m^{H_2O} = \begin{cases} k_{\text{cond}}\varepsilon(1-s)\dfrac{M^{H_2O}p_g}{RT}(x_g^{H_2O} - x_{\text{sat}}^{H_2O}) & \text{if } x_g^{H_2O} \geq x_{\text{sat}}^{H_2O} \\ k_{\text{vap}}\varepsilon s\rho_l p_g(x_g^{H_2O} - x_{\text{sat}}^{H_2O}) & \text{if } x_g^{H_2O} < x_{\text{sat}}^{H_2O} \end{cases} \tag{45}$$

here factors $(1-s)$ and s are introduced to account for the variation of the interfacial mass transfer with liquid water saturation, k_{cond} and k_{vap} are the water vapour condensation rate and the liquid water evaporation rate, respectively, $x_g^{H_2O}$ is the molar fraction of water vapour, $x_{\text{sat}}^{H_2O}$ is the saturation molar fraction of water vapour and related to the temperature by [14],

$$x_{\text{sat}}^{H_2O}(T, 1\text{ atm}) = 10^{(28.59051 - 8.2\log_{10}(T) + 0.0024804T - 3142.31/T)} \tag{46}$$

The effective diffusion coefficients of water vapour and oxygen are estimated respectively using Bruggeman relation,

$$D_{g,\text{eff}}^{H_2O} = \varepsilon^{1.5}D_g^{H_2O} \tag{47}$$

$$D_{g,\text{eff}}^{O_2} = \varepsilon^{1.5}D_g^{O_2} \tag{48}$$

and the bulk diffusivities are temperature dependent and given by [2]

$$D_g^{H_2O} = 0.256 \times 10^{-4} \times \left(\frac{T}{307.15}\right)^{2.334} \tag{49}$$

$$D_g^{O_2} = 0.1775 \times 10^{-4} \times \left(\frac{T}{273.15}\right)^{1.823} \tag{50}$$

A fitted relation is employed to reflect the dependence of the enthalpy of water vaporization H_{vap} ($J\,kg^{-1}$) on temperature based on the data provided in [22].

$$H_{\text{vap}} = 3.0709 \times 10^5(647.15 - T)^{0.35549} \tag{51}$$

The specific heat capacity of liquid water as a function of temperature is fitted based on the figure provided in [23]

$$\begin{aligned} c_l = &-4.0699 \times 10^{-8}(T-273.15)^5 + 1.3113 \\ &\times 10^{-5}(T-273.15)^4 - 1.6290 \times 10^{-3}(T-273.15)^3 \\ &+ 1.0536 \times 10^{-1}(T-273.15)^2 \\ &- 3.2989(T-273.15) + 4216.4 \end{aligned} \tag{52}$$

The specific heat capacities for oxygen, nitrogen and water vapour are also temperature dependent and given in [23] as

$$c_g^{O_2} = \frac{R}{M^{O_2}}(3.068 + 1.638 \times 10^{-3}T - 0.512 \times 10^{-6}T^2) \tag{53}$$

$$c_g^{N_2} = \frac{R}{M^{N_2}}(3.247 + 0.712 \times 10^{-3}T - 0.041 \times 10^{-6}T^2) \tag{54}$$

$$c_g^{H_2O} = \frac{R}{M^{H_2O}}(3.634 + 1.195 \times 10^{-3}T + 0.135 \times 10^{-6}T^2) \tag{55}$$

The specific heat capacity of the gas phase is estimated as

$$c_g = c_g^{O_2}C_g^{O_2} + c_g^{H_2O}C_g^{H_2O} + c_g^{N_2}(1 - C_g^{O_2} - C_g^{H_2O}) \tag{56}$$

Similarly, the thermal conductivity of the gas phase is estimated by

$$k_g = k_g^{O_2}C_g^{O_2} + k_g^{H_2O}C_g^{H_2O} + k_g^{N_2}(1 - C_g^{O_2} - C_g^{H_2O}) \tag{57}$$

The molar fraction of each species is related to its mass fraction by

$$x_g^j = C_g^j \frac{M_g}{M^j} \tag{58}$$

$$\sum_j x_g^j = 1 \tag{59}$$

where $j = O_2, H_2O, N_2$. Therefore, the molar mass of the gas phase can be calculated by

$$M_g = \left(\sum_j \frac{C_g^j}{M^j} \right)^{-1} \tag{60}$$

As in [14], by keeping $x_g^{O_2}/x_g^{N_2} = 21/79$ at the cathode GDL/channel interface, the mass fractions of water vapour and oxygen at the interface can be determined by the relative humidity

$$x_{g,L}^{H_2O} = RH \cdot x_{sat,L}^{H_2O} \tag{61}$$

$$x_{g,L}^{O_2} = \frac{1 - x_{g,L}^{H_2O}}{1 + 79/21} \tag{62}$$

Therefore, the mass fractions of water vapour and oxygen, and molar mass of the gas phase at the cathode GDL/channel interface can be calculated as

$$C_{g,L}^{H_2O} = x_{g,L}^{H_2O} \frac{M^{H_2O}}{M_{g,L}} \tag{63}$$

$$C_{g,L}^{O_2} = x_{g,L}^{O_2} \cdot \frac{M^{O_2}}{M_{g,L}} \tag{64}$$

$$M_{g,L} = x_{g,L}^{O_2} M^{O_2} + x_{g,L}^{H_2O} M^{H_2O} + (1 - x_{g,L}^{O_2} - x_{g,L}^{H_2O}) M^{N_2} \tag{65}$$

3. Results and discussion

The parameter values used in the base case are listed in Table 1. In order to investigate the effect of various parameters on the transient or steady behaviour of different species in the cathode GDL, four parameters (the liquid water saturation at the GDL/channel interface (s_L), the percentage of liquid water to all the water at the CL/GDL interface (β), the current density (i_c), and the wetting angle (θ_c)) are chosen to be varied. The time needed for the liquid water saturation to reach steady state is defined similar as in [24],

$$t_{steady} = \max_t \left\{ abs \left(\frac{\int_0^L s(t,x)\,dx - \int_0^L s(t+\Delta t, x)\,dx}{\int_0^L s(t,x)\,dx} \right) \leq 1e-5 \right\} \tag{66}$$

where Δt is the time step used in the numerical simulation.

Table 1
Parameter values for base case

ε	0.4
ρ_l (kg m^{-3})	983
μ_g (kg m^{-1} s^{-1})	1.9×10^{-5} [14]
K (m^2)	7×10^{-13} [14]
k_{cond} (s^{-1})	100 [1]
k_{vap} (N^{-1} m^2 s^{-1})	1/101325
M^{H_2O} (kg mol^{-1})	1.8×10^{-2}
M^{O_2} (kg mol^{-1})	3.2×10^{-2}
M^{N_2} (kg mol^{-1})	2.8×10^{-2}
R (J mol^{-1} K^{-1})	8.315
s_0	0
s_L	0
i_c (A m^{-2})	10000
F (C mol^{-1})	96487
α	0.25 [14]
p_L^g (N m^{-2})	101325
$C_l^{H_2O}$	1
σ (N m^{-1})	6.25×10^{-2} [14]
θ_c ($^\circ$)	110 [14]
RH (%)	95
k_l (W m^{-1} K^{-1})	0.58 [25]
$k_g^{O_2}$ (W m^{-1} K^{-1})	0.024 [25]
$k_g^{N_2}$ (W m^{-1} K^{-1})	0.024 [25]
$k_g^{H_2O}$ (W m^{-1} K^{-1})	0.016 [25]
k_s (W m^{-1} K^{-1})	1.7 [25]
c_s (J kg^{-1} K^{-1})	709 [25]
ρ_s (kg m^{-3})	2267 [25]
T_L (K)	333
ΔS_c^{Pt} (J mol^{-1} K^{-1})	-326.36 [14]
σ_c (S m^{-1})	1900 [14]
ζ_1 (A m^{-2})	0.12 [14]
ζ_2 (V^{-1})	30.6 [14]
β	0.5
L (m)	3×10^{-4}

3.1. The effect of s_L

The parameter, s_L, is the liquid water saturation specified as a boundary condition at the GDL/channel interface. Fig. 2 shows the change of the distribution of the liquid water saturation in the GDL with time. When $s_L = 0$ (the baseline case), implying no liquid water exists at the GDL/channel interface, the transient behaviour of the liquid water saturation is shown in Fig. 2(a). At $t = 0$, no liquid water in the GDL, that is, $s(t, x)|_{t=0} \equiv 0$, is assumed. Thereafter, liquid water starts to accumulate at the cathode CL/GDL interface and seeps gradually from the CL/GDL interface ($x = 0$) to the GDL/channel interface ($x = L$) because of the capillary pressure. It takes about 14.5 s for liquid water to reach its steady state. The highest water saturation is about 0.077 at the cathode CL/GDL interface. When $s_L = 0.05$ and $s|_{t=0} = 0$, liquid water comes from both sides of the GDL and meets at a point close to the GDL/channel interface as shown in Fig. 2(b). Water saturation then increases across the entire GDL thickness and reaches its steady state after about 11.59 s. At steady state, the water saturation at $x = 0$ reaches to 0.081. When s_L is specified as 0.1 or 0.15 and $s|_{t=0} = 0$, similar to the case of $s_L = 0.05$, liquid water seeps first from both sides of the GDL and then meets at a point close to the CL/GDL interface as indicated in Fig. 2(c) and (d). The time needed for the
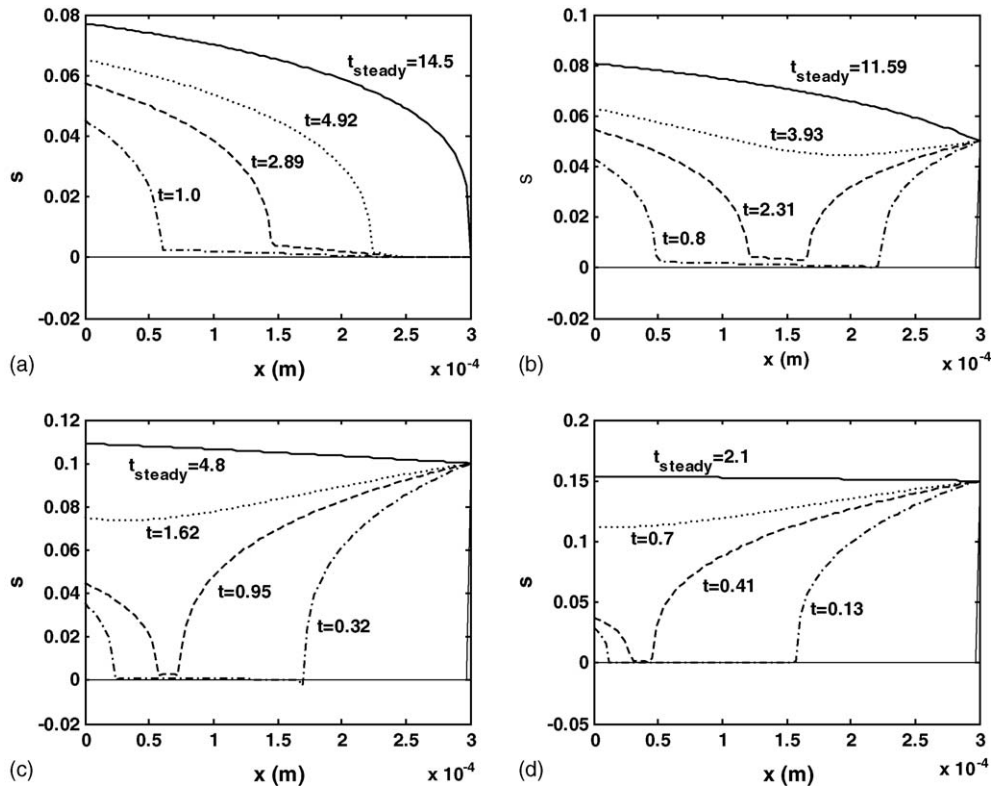
Fig. 2. The effect of water saturation at $x=L$ on the transient behaviour of water saturation in the cathode GDL. (a) $s_L=0$, (b) $s_L=0.05$, (c) $s_L=0.1$, (d) $s_L=0.15$.

water saturation to reach steady state is further reduced to 4.8 and 2.1 s and the water saturation at $x=0$ is 0.109 and 0.154, respectively. The water saturation distribution at steady state is a linear-like function through the thickness of the GDL and a little bit higher at $x=0$ than at $x=L$ when liquid water saturation is higher than 0.1, which is shown by the solid line in Fig. 2(c) and (d).

By comparing Fig. 2(a)–(d), it can be seen that the water saturation at the cathode CL/GDL interface increases with an increase of the water saturation at the cathode GDL/channel interface, and meanwhile, the time needed for water saturation to reach steady state decreases. This phenomenon is also clearly reflected in Fig. 3.

Fig. 4 gives the mass transfer rate distribution across the thickness of the GDL at steady state for the four cases, $s_L=0$, 0.05, 0.1 and 0.15. $m^{H_2O} > 0$ means water vapour condensation takes place and $m^{H_2O} < 0$ implies liquid water evaporation occurs. In the baseline case (Fig. 4(a)), water condensation takes place in the most portion of the GDL close to the CL/GDL interface side due to high water vapour concentration in this region (see Fig. 5(b)). Water evaporation happens only in a small portion of the GDL close to the GDL/channel side because of a relatively low water vapour concentration within this side (see Fig. 5(b)). Fig. 4(b)–(d) indicate that when s_L value goes up, the mass transfer close to the GDL/channel interface is in favour of evaporation and the rate goes down accordingly.

The time needed for water vapour, oxygen, gas phase pressure, and temperature to reach steady state are usually very short (<0.2 s), so their transient behaviours are not as important as liq-

uid water and thus omitted here. But their steady state behaviours are presented hereafter.

Fig. 5 depicts the steady state distributions of gas phase pressure, water vapour concentration, oxygen concentration and temperature across the thickness of the cathode GDL at different levels of liquid water saturation at $x=L$. It can be seen that the change of s_L value has a slight effect on the gas phase pressure drop and the temperature increase within the GDL from the channel side to the CL side, as shown in Fig. 5(a) and (d). The gas phase pressure drop is about 2.3 Pa while the temperature increase is about 1.3 °C. Fig. 5(b) and (c) shows that an increase
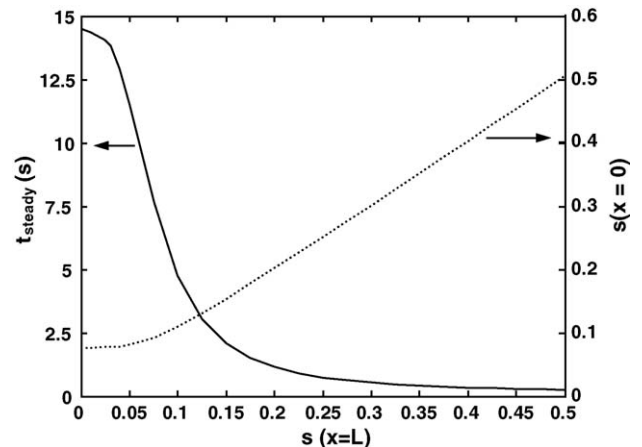

Fig. 3. The effect of water saturation at $x=L$ on the time needed for water saturation to reach steady state and on the water saturation at $x=0$.
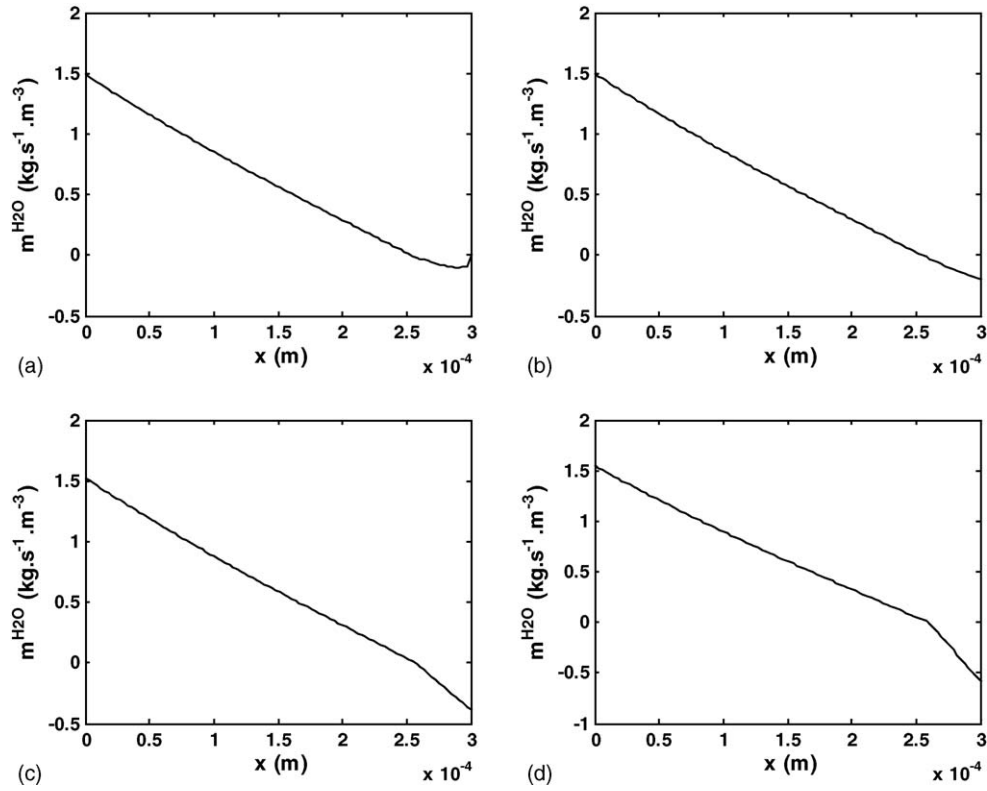
Fig. 4. Mass transfer rate at steady state for different water saturation at $x = L$. (a) $s_L = 0$, (b) $s_L = 0.05$, (c) $s_L = 0.1$, (d) $s_L = 0.15$.
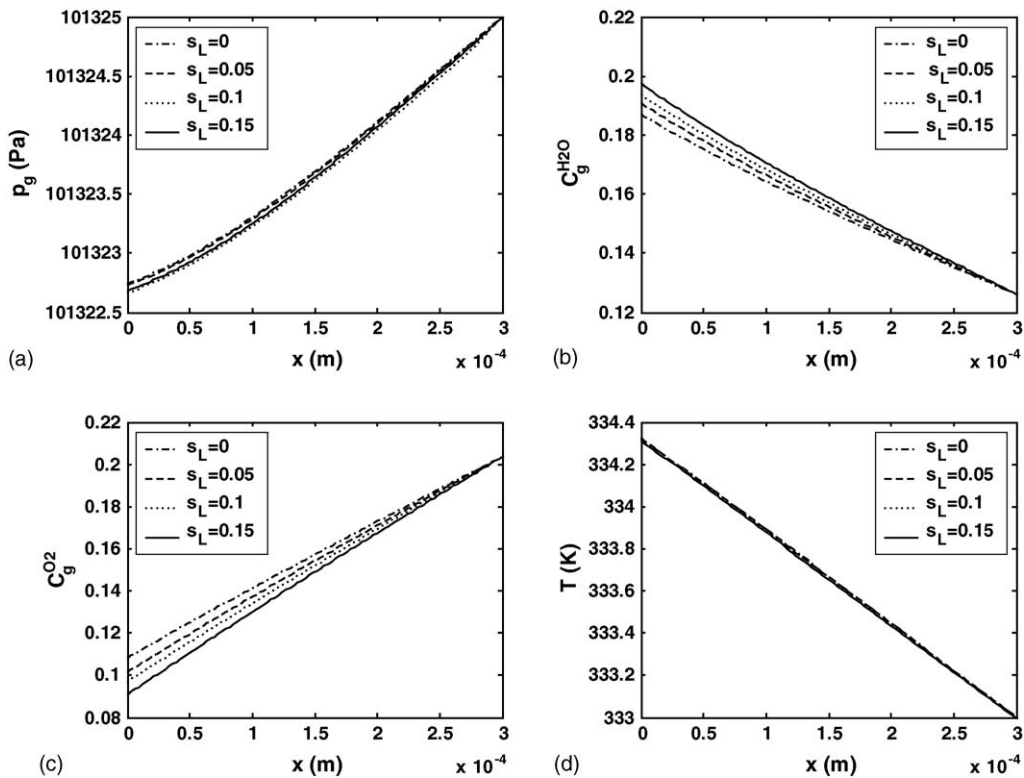

Fig. 5. The effect of water saturation at $x = L$ on the steady state distribution of (a) water vapour concentration, (b) oxygen concentration, (c) gas phase pressure, and (d) temperature.
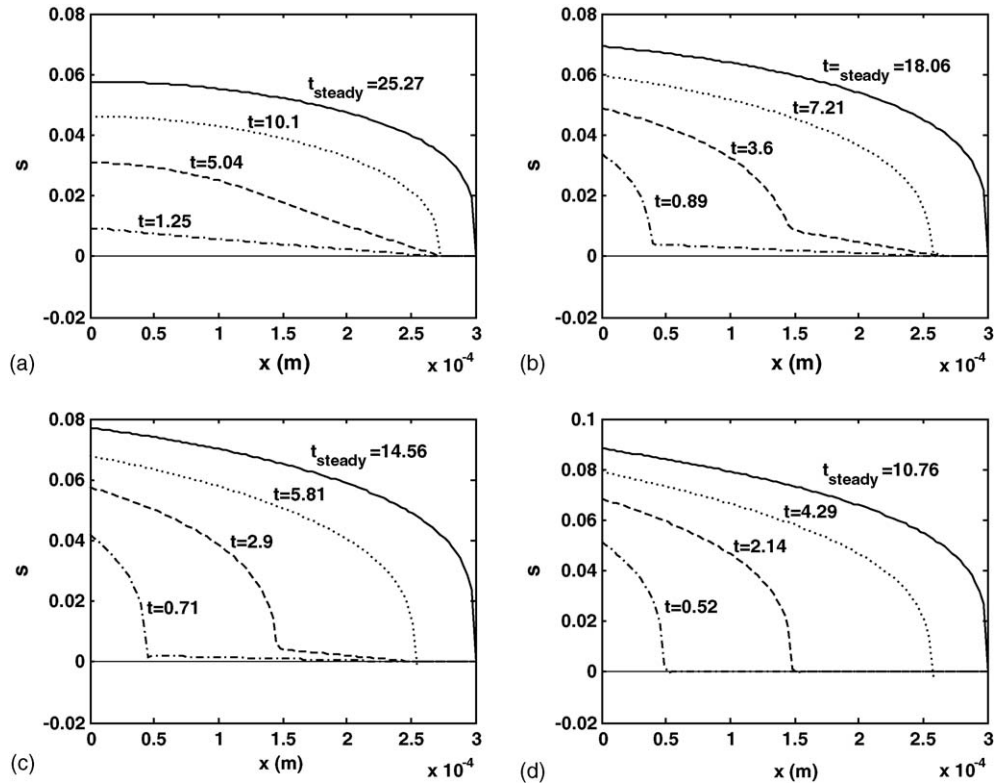
Fig. 6. The effect of parameter β on the transient behaviour of water saturation in the cathode GDL. (a) $\beta = 0$, (b) $\beta = 0.25$, (c) $\beta = 0.5$, (d) $\beta = 1.0$.

of s_L value will result in a higher water vapour concentration and a lower oxygen concentration across the thickness of the cathode GDL.

3.2. The effect of β

It is unclear at this stage that how much liquid water and how much water vapour enters the GDL from the cathode CL side. In this paper, a parameter β is introduced to account for the liquid water percentage to all of the water at the cathode CL/GDL interface. Fig. 6 shows the effect of parameter β on the transient behaviour of liquid water saturation in the cathode GDL. If all of the water at the cathode CL/GDL interface is in vapour form, that is, $\beta = 0$, the water vapour concentration is greater than its saturation value $x_{sat}^{H_2O}$ and as a result, it condenses into liquid form. Therefore, liquid water saturation gradually increases from the CL side to the channel side and finally reaches its steady state where liquid water pressure and gas phase pressure are balanced by the capillary pressure ($p_c = p_g - p_l$). The whole process takes about 25.27 s and the maximum liquid water saturation is about 0.058 at the cathode CL/GDL interface, as shown in Fig. 6(a). If the value of the parameter β is respectively increased from 0 to 0.25, 0.5 and 1.0, meaning that more liquid water enters the GDL from the CL side, liquid water saturations at steady state are also increased, as shown in Fig. 6(b)–(d), and the time needed for liquid water saturation to reach steady state is correspondingly reduced from 25.27 to 18.06, 14.56 and 10.76 s, respectively. At the steady state, the liquid water saturation at the

CL/GDL interface associated with $\beta = 0.25$, 0.5 and 1.0 reaches 0.069, 0.077 and 0.088, respectively.

The variations of the time needed for liquid water saturation to reach steady state and the water saturation at the CL/GDL interface with the parameter β are plotted in Fig. 7. It can be seen that a higher β value results in a shorter time needed for water saturation to reach steady state and higher liquid water saturation at the CL/GDL interface.

Fig. 8 gives the mass transfer rate distributions in the GDL at steady state for $\beta = 0.0$, 0.25, 0.5 and 1.0, respectively. Though
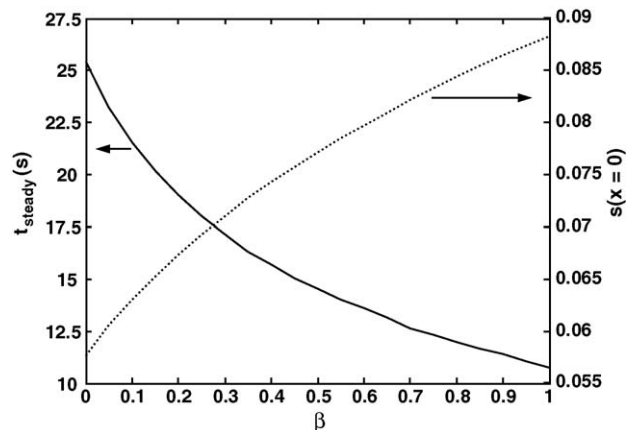

Fig. 7. The effect of parameter β on the time needed for water saturation to reach steady state and on the water saturation at $x = 0$.
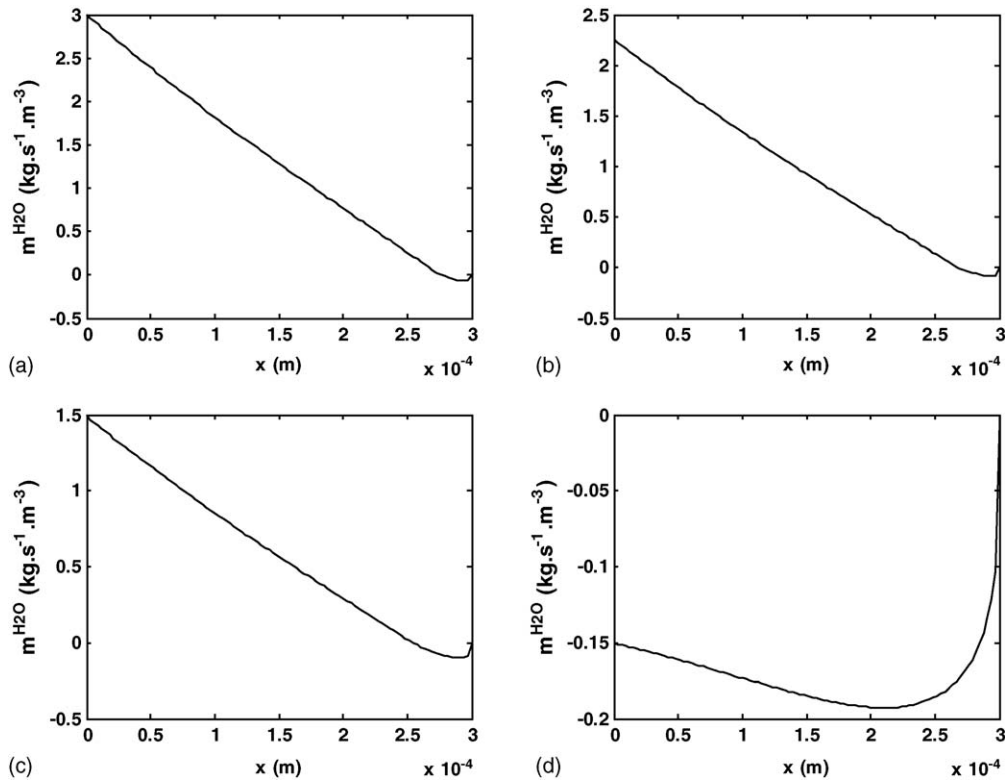
Fig. 8. Mass transfer rate at steady state. (a) $\beta = 0$, (b) $\beta = 0.25$, (c) $\beta = 0.5$, (d) $\beta = 1.0$.

the interplay among phase change, pressure, temperature and boundary conditions is very complex, some quantitative and qualitative predictions can be carried out using the set of models given above. Under the given initial and boundary conditions, it can be seen from Fig. 8(a)–(c) that water vapour condensation usually takes place near the CL side and evaporation occurs near the channel side because of the water vapour concentration is greater than its saturation value near the CL side and less than its saturation value near the channel side. The dividing point between condensation and evaporation moves from the channel side to the cathode CL side when β increases. But when β is very close to 1, say $0.95 < \beta < 1$, condensation process does not happen and only evaporation takes place, as shown in Fig. 8(d), because too much liquid water exists and water vapour concentration through the whole GDL does not reach its saturation level.

The steady state distributions for gas phase pressure, water vapour concentration, oxygen concentration and temperature in the GDL at different β values are given in Fig. 9. Noting that, when $\beta = 0$ and 0.25, the gas phase pressure at the CL/GDL interface is higher than the pressure at the GDL/channel interface due to the higher water vapour concentration at the CL/GDL interface, as shown in Fig. 9(a). The gas phase pressure begins to drop from the channel side to the CL side when the β value becomes bigger ($\beta = 0.5$ and 1 in Fig. 9(a)). The water vapour concentration decreases with the increase of β value, as shown in Fig. 9(b), which leads to a high oxygen concentration distribution (Fig. 9(c)) because of the less convection effect of water vapour on the oxygen transport in the GDL. Furthermore, it can

be seen from Fig. 9(d) that a bigger β value will reduce the temperature difference between the both sides of the GDL.

3.3. The effect of i_c

The water saturation distributions at different times are plotted in Fig. 10 for four current densities, $i_c = 1000, 2000, 5000$ and 10,000 A m^{-2}. A higher current density implies more water produced through the electrochemical reaction in the cathode CL and more oxygen is consumed. Therefore, more liquid water and water vapour come into the cathode GDL from the CL/GDL interface that results in a high liquid water saturation distribution through the thickness of the GDL, as shown in Fig. 10(a)–(d). The maximum liquid water saturation for each current density is found at the CL/GDL interface and is increased from 0.039 for $i_c = 1000$ A m^{-2} to 0.049, 0.064, and 0.077, respectively, for $i_c = 2000, 5000$ and 10,000 A m^{-2}. The time needed for liquid water saturation to reach steady state is down from 76.37 s for $i_c = 1000$ A m^{-2} to 45.73, 23.42, and 14.56 s for $i_c = 2000, 5000$ and 10,000 A m^{-2}, respectively.

The effect of the current density on the time needed for water saturation to reach steady state and on the water saturation at the CL/GDL interface are shown in Fig. 11. It can be seen that increasing the working current density reduces the time for liquid water to reach steady state but increases the liquid water saturation at the CL/GDL interface.

Fig. 12 gives the mass transfer rate distributions at steady state for the four cases corresponding to $i_c = 1000, 2000, 5000$ and 10,000 A m^{-2}, respectively. It can be seen that at low current
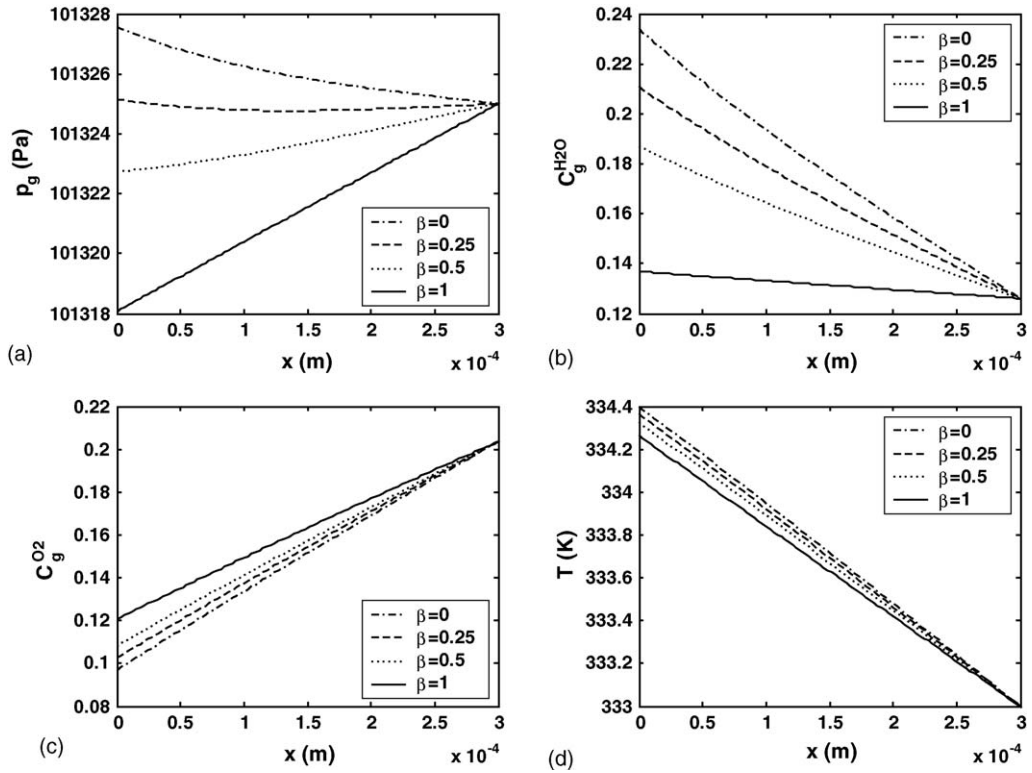
Fig. 9. The effect of parameter β on the steady state distribution of (a) water vapour, (b) oxygen, (c) gas phase pressure, and (d) temperature.
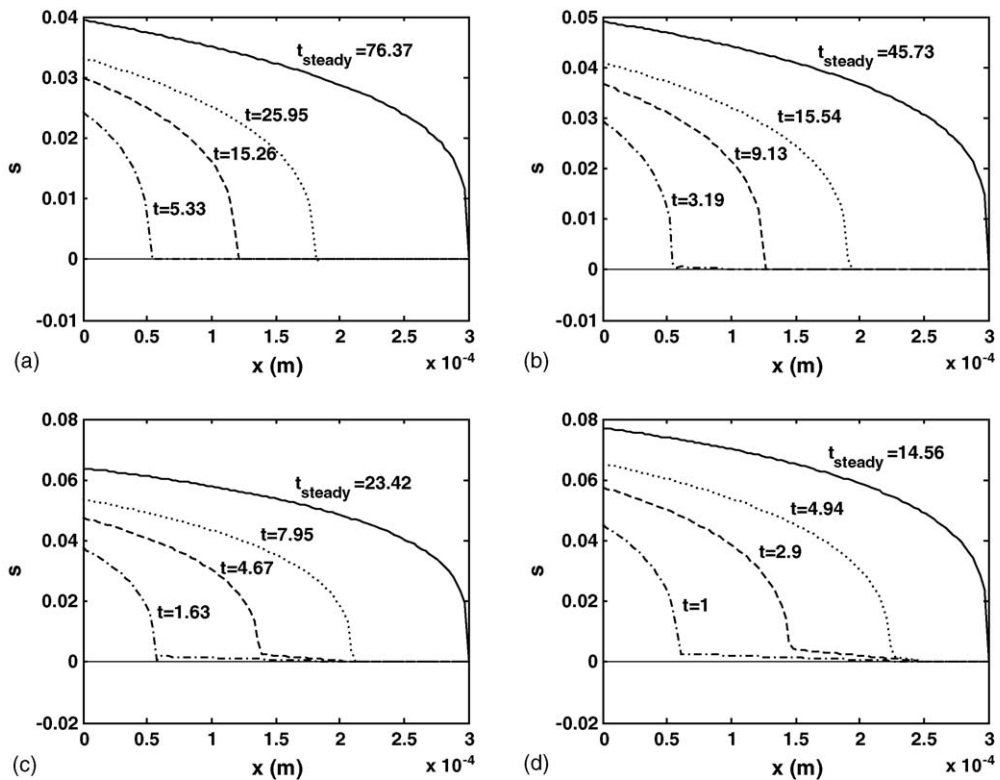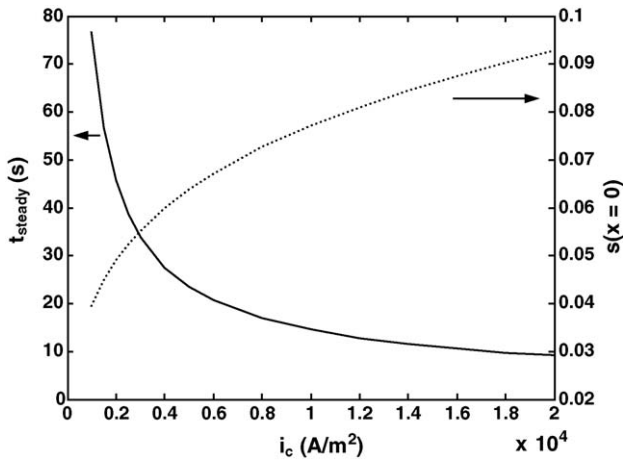

Fig. 10. The effect of the current density on the transient behaviour of water saturation in the cathode GDL. (a) $i_c = 1000 \, \text{A m}^{-2}$, (b) $i_c = 2000 \, \text{A m}^{-2}$, (c) $i_c = 5000 \, \text{A m}^{-2}$, (d) $i_c = 10,000 \, \text{A m}^{-2}$.

Fig. 11. The effect of the current density on the time needed for water saturation to reach steady state and on the water saturation at $x = 0$.

density, as shown in Fig. 12(a) and (b), evaporation dominates the phase change process of water in a large portion of the GDL close to the GDL/channel interface while condensation takes place only in a small portion of the GDL close to the CL/GDL interface. The reason is that at low current density water vapour enters into the GDL from the CL side and is oversaturated in a small portion of the GDL close to the CL/GDL interface side resulting in the water vapour condensation in this part. On the other hand, the most part of the GDL close to the GDL/channel interface side is unsaturated, resulting in the liquid water evaporation. With the increasing of the current density, more and more liquid water enters into the GDL resulting in the water

vapour in the most part of the GDL from the left side to the right side over saturated, and gradually, water vapour condensation replaces evaporation becoming the major process for the phase change in the GDL, as shown in Fig. 10(c) and (d).

The distributions for gas phase pressure, water vapour concentration, oxygen concentration and temperature through the thickness of the cathode GDL are shown in Fig. 13. It can be seen that increasing the current density will increase the gas phase pressure drop in the GDL, and lower the oxygen concentration, but will increase the water vapour concentration and the temperature difference between the two sides of the GDL.

3.4. The effect of θ_c

Fig. 14 shows the dynamic behaviours of liquid water saturation in the GDL versus the four different contact angles, $\theta_c = 0, 70, 110$ and $150\,^{\circ}\mathrm{C}$. The first two cases correspond to hydrophilic GDLs and the last two represent hydrophobic GDLs. The shape of the water saturation distribution across the thickness of the GDL seems not affected too much by the contact angle of the GDL but the values change a lot. For hydrophilic GDLs ($\theta_c < 90\,^{\circ}\mathrm{C}$), a bigger contact angle implies that the GDL tends to hold more water so a higher steady state distribution of liquid water saturation is expected, Fig. 14(a) and (b); for hydrophobic GDLs ($\theta_c > 90\,^{\circ}\mathrm{C}$), adverse tendency is observed, i.e., increasing the contact angle will reduce the ability of the GDL to hold more water and results in a lower steady state distribution of liquid water saturation, Fig. 14(c) and (d). In addition, the time needed for water saturation to reach steady state will
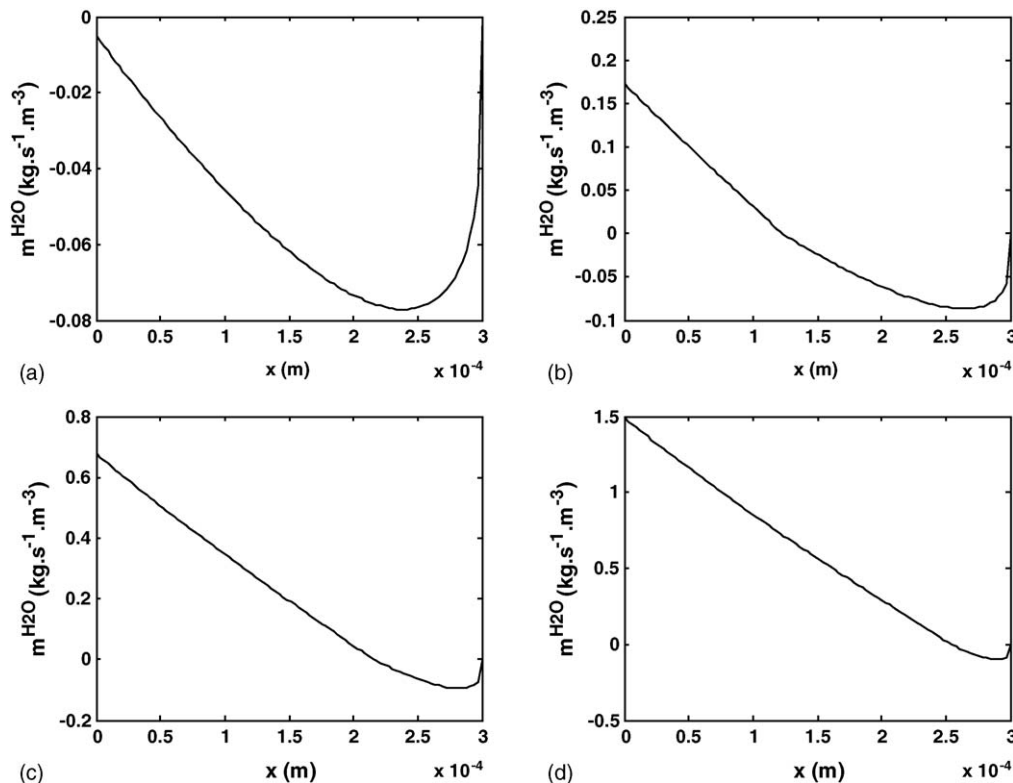

Fig. 12. Mass transfer rate at steady state for different current densities. (a) $i_c = 1000\,\mathrm{A\,m^{-2}}$, (b) $i_c = 2000\,\mathrm{A\,m^{-2}}$, (c) $i_c = 5000\,\mathrm{A\,m^{-2}}$, (d) $i_c = 10{,}000\,\mathrm{A\,m^{-2}}$.
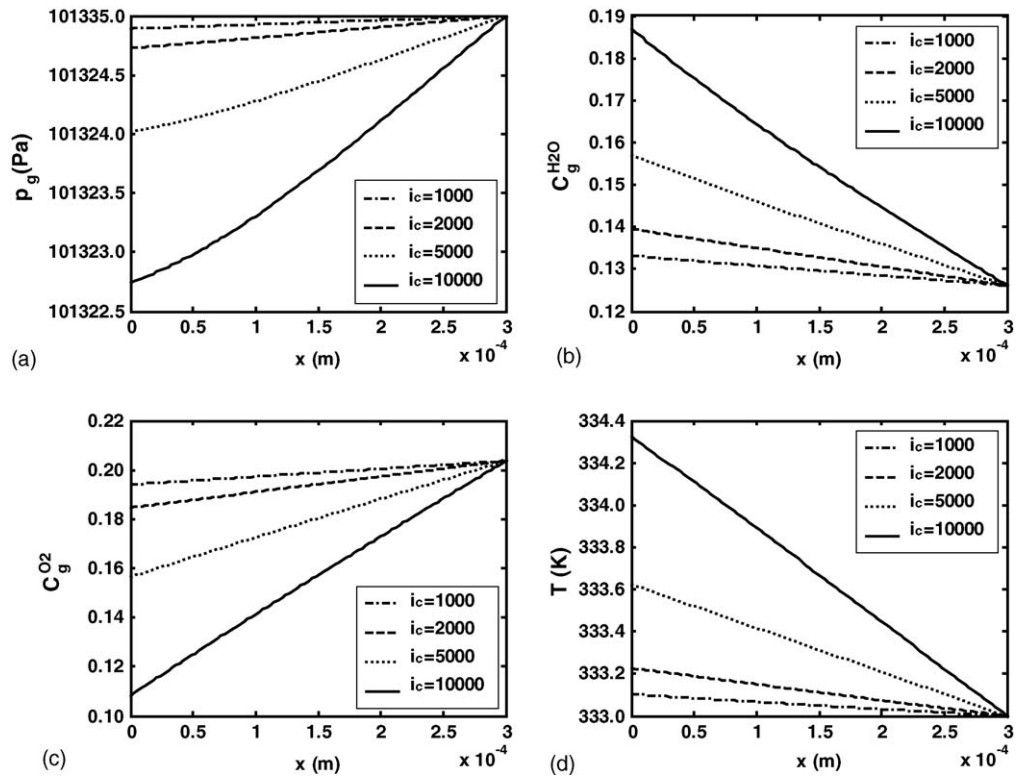
Fig. 13. The effect of the current density on the steady state distribution of (a) water vapour, (b) oxygen, (c) gas phase pressure, and (d) temperature.
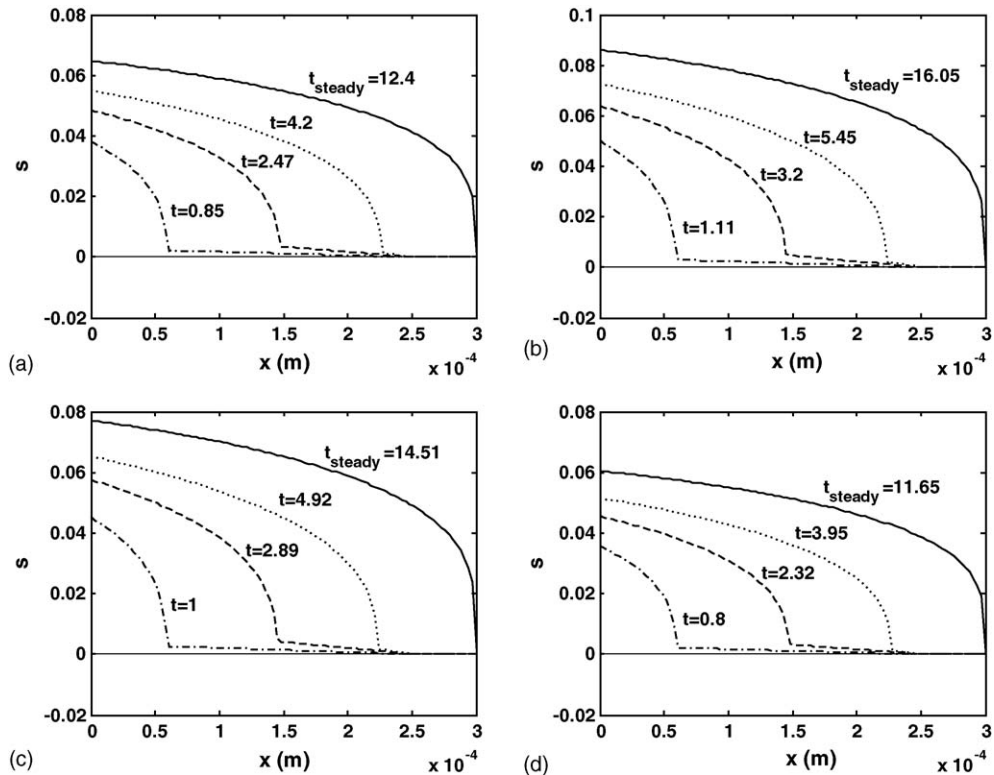

Fig. 14. The effect of the contact angle on the transient behaviour of water saturation in the cathode GDL. (a) $\theta_c = 0\,^\circ$C, (b) $\theta_c = 70\,^\circ$C, (c) $\theta_c = 100\,^\circ$C, (d) $\theta_c = 150\,^\circ$C.
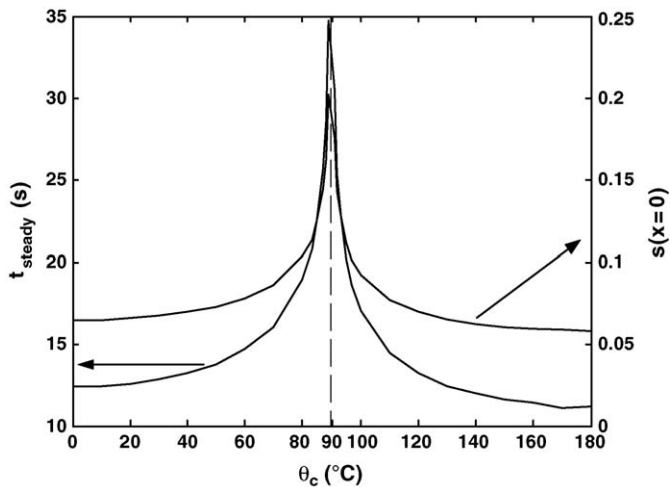
Fig. 15. The effect of the contact angle on the time needed for water saturation to reach steady state and on the water saturation at $x = 0$.

increase when the contact angle increases for hydrophilic GDLs while the time will decrease when the contact angle increases for hydrophobic GDLs. The same trend is also observed for the liquid water saturation at the cathode CL/GDL interface. These phenomena are well reflected in Fig. 15. The more the contact angle closes to 90 °C, the longer the time needed for water saturation to reach steady state and the higher the water saturation at the interface of the cathode CL/GDL are. The steady state mass transfer rate and distributions of water vapour, oxygen, gas phase pressure and temperature are almost unchanged for the four contact angles and so their figures are not presented here.

4. Conclusions

The transient dynamics of water transport in the cathode gas diffusion layer of PEM fuel cells is studied based on a one-dimensional, two-phase, nonisothermal transient model. According to the numerical simulations, it can be concluded as follows:

1. When the water saturation at the cathode GDL/channel interface is big enough (≥ 0.1) liquid water is almost uniformly distributed across the thickness of the cathode GDL at steady state. Increase the water saturation at the GDL/channel interface will increase the entire water saturation in the whole GDL and reduce the time needed for liquid water saturation to reach steady state. In order to obtain a high oxygen concentration at the CL/GDL interface, the water saturation at the GDL/channel interface should be kept as low as possible.
2. More liquid water and less water vapour at the CL/GDL interface are helpful to reduce the time needed for liquid water

saturation to reach steady state and helpful for the oxygen transport. Water vapour condensation takes place in the GDL near the CL side and liquid water evaporation occurs near the channel side. This conclusion depends strongly on the boundary conditions at the GDL/channel interface.
3. At low current density range, evaporation dominates the water phase change; but at high current density range, condensation is the major process for water phase change in the cathode GDL. Increasing the current density will reduce the time needed for water saturation to reach steady state and increase the water saturation at the CL/GDL interface.
4. For hydrophilic GDLs ($\theta_c < 90$ °C), when the contact angle increases both the time needed for liquid water saturation to reach steady state and the water saturation at the interface of the CL/GDL increase and attain their maximum point around 90 °C; for hydrophobic GDLs ($\theta_c > 90$ °C), both of them decrease when the contact angle increases.

References

[1] W. He, J.S. Yi, T.V. Nguyen, AIChE J. 46 (2000) 2053–2064.
[2] G. Lin, W. He, T.V. Nguyen, J. Electrochem. Soc. 151 (2004) A1999–A2006.
[3] G.J.M. Janssen, J. Electrochem. Soc. 148 (2001) A1313–A1323.
[4] Z.H. Wang, C.Y. Wang, K.S. Chen, J. Power Sources 94 (2001) 40–50.
[5] C.Y. Wang, P. Cheng, Int. J. Heat Mass Transfer 39 (1996) 3607–3618.
[6] L. You, H. Liu, Int. J. Heat Mass Transfer 45 (2002) 2277–2287.
[7] S. Mazumder, J.V. Cole, J. Electrochem. Soc. 150 (2003) A1510–A1517.
[8] T. Berning, N. Djilali, J. Electrochem. Soc. 150 (2003) A1589–A1598.
[9] J.H. Nam, M. Kaviany, Int. J. Heat Mass Transfer 46 (2003) 4595–4611.
[10] U. Pasaogullari, C.Y. Wang, J. Electrochem. Soc. 152 (2005) A380–A390.
[11] A.Z. Weber, R.M. Darling, J. Newman, J. Electrochem. Soc. 151 (2004) A1715–A1727.
[12] U. Pasaogullari, C.Y. Wang, J. Electrochem. Soc. 151 (2004) A399–A406.
[13] M. Noponen, E. Birgersson, J. Ihonen, M. Vynnycky, A. Lundblad, G. Lindbergh, Fuel Cells 4 (2004) 365–377.
[14] E. Birgersson, M. Noponen, M. Vynnycky, J. Electrochem. Soc. 152 (2005) A1021–A1034.
[15] D. Natarajan, T.V. Nguyen, J. Electrochem. Soc. 148 (2001) A1324–A1335.
[16] M. Ceraolo, C. Miulli, A. Pozio, J. Power Sources 113 (2003) 131–144.
[17] J.C. Amphlett, R.F. Mann, B.A. Peppley, P.R. Roberge, A. Rodrigues, J. Power Sources 61 (1996) 183–188.
[18] D. Natarajan, T.V. Nguyen, J. Power Sources 115 (2003) 66–80.
[19] Y. Wang, C.Y. Wang, Electrochim. Acta 50 (2005) 1307–1315.
[20] L.M. Abriola, G.F. Pinder, Water Resour. Res. 21 (1985) 11–18.
[21] M.J. Lampinen, M. Fomino, J. Electrochem. Soc. 140 (1993) 3537–3546.
[22] K.N. Marsh, Recommended Reference Materials for the Realization of Physicochemical Properties, Blackwell Scientific Publications, Oxford, 1987.
[23] M.W. Zemansky, R.H. Dittman, Heat Thermodynamics, 6th ed., McGraw-Hill, 1981.
[24] F. Chen, Y.G. Su, C.Y. Soong, W.M. Yan, H.S. Chu, J. Electroanal. Chem. 566 (2004) 85–93.
[25] The Engineering Tool Box, http://www.engoneeringtoolbox.com/, 2005.